

Article

# Selectivity Dependence of 1,1-Difluoro-1-Chloroethane Dehydrohalogenation on the Metal–Support Interaction over SrF<sub>2</sub> Catalyst

Wucan Liu <sup>1</sup>, Yongnan Liu <sup>2</sup>, Kabozya M. Mardochee <sup>2</sup>, Zhikun Wang <sup>2</sup>, Shucheng Wang <sup>1</sup>, Wei Yu <sup>2</sup> , Jianjun Zhang <sup>1</sup> and Wenfeng Han <sup>2,\*</sup> 

<sup>1</sup> State Key Laboratory of Fluorinated Greenhouse Gases Replacement and Control Treatment, Zhejiang Research Institute of Chemical Industry, Tianmushan Road 387, Hangzhou 310032, China; liuwucan@sinochem.com (W.L.); wangshucheng1@sinochem.com (S.W.); zhangjianjun@sinochem.com (J.Z.)

<sup>2</sup> Institute of Industrial Catalysis, Zhejiang University of Technology, Chaowang Road 18, Hangzhou 310014, China; Yongnan\_Liu@126.com (Y.L.); cheizymaww@163.com (K.M.M.); Wangzk\_ZJUT@126.com (Z.W.); WillYmt1989@outlook.com (W.Y.)

\* Correspondence: hanwf@zjut.edu.cn

Received: 10 March 2020; Accepted: 22 March 2020; Published: 23 March 2020



**Abstract:** SrF<sub>2</sub> promotes the dehydrochlorination (DeHCl) of 1,1-difluoro-1-chloroethane, which is the key process for the manufacture of VDF (vinylidene fluoride), one of the most typical fluorinated monomers. However, the selectivity is low as dehydrofluorination (DeHF) to VCF (vinylidene chlorofluoride) competes with the formation of VDF. In this study, SrF<sub>2</sub>@C (SrF<sub>2</sub> embedded in carbon) and SrF<sub>2</sub>@NC (N-doped carbon) catalysts were fabricated following calcination in N<sub>2</sub> with SrC<sub>2</sub>O<sub>4</sub>, PVDF (poly vinylidene fluoride) and urea as the precursors. The catalysts were characterized by XRD, SEM, TEM, and XPS. The results show that both the calcination temperature and N-doping play an important role in the conversion of HCFC-142b and the selectivity to VDF and VCF. Calcination at elevated temperatures enhances the Sr-C interaction. For SrF<sub>2</sub>@C, improved interaction facilitates withdrawing electrons from Sr by the carbon support. By contrast, the strong interaction of Sr with N-doped carbon supply electrons from N species to Sr. The electron deficiency of Sr is favorable for the adsorption of F with higher electronegativity and consequently, DeHF reaction forming VCF. The supply of electrons to Sr by the support improves the formation of VDF (DeHCl). The present work provides a potential strategy for the improvement of selectivity to the target product.

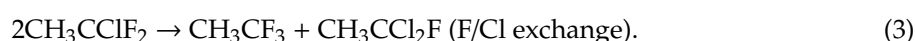
**Keywords:** dehydrochlorination; dehydrofluorination; metal–support interaction; strontium fluoride; vinyl difluoride

## 1. Introduction

Vinylidene fluoride (VDF, CH<sub>2</sub>=CF<sub>2</sub>) is one of most important fluorine-containing monomers and the raw material for the preparation of various fluorine elastomers and fluorocarbon coating materials [1,2]. At present, VDF is mainly prepared by the pyrolysis of 1,1-difluoro-1-chloroethane (HCFC-142b). As two fluorine atoms are connected to one carbon atom in HCFC-142b, the bond energy of the C-Cl bond is enhanced [3]. Thus, pyrolysis of HCFC-142b requires high temperatures in the absence of catalysts. In industry, VDF is prepared by thermal decomposition of HCFC-142b at high temperatures (>650 °C). The main problems of thermal decomposition include the high temperature, high energy consumption, and serious coke deposition. To reduce the reaction temperature and coke formation, CO<sub>2</sub> and steam were suggested as the dilution gases [4]. With large amounts of dilution gas, the cost of separation is increased significantly. In addition, numerous waste-water is also produced.

Proper catalysts for the pyrolysis of 1,1-difluoro-1-chloroethane significantly reduce the reaction temperature and carbon deposition. In our previous studies, we discovered that pyrolysis of HCFC-142b is catalyzed by materials such as N-doped activated carbon [5], N-containing mesoporous carbon [6], and metal fluorides [7]. The adoption of catalysts lowers the reaction temperature from 650 °C to 350 °C. Consequently, the energy consumption can be saved significantly. In addition, the coke formation is decreased significantly at low reaction temperatures. Except for the moderate conversion levels, both N-doped activated carbon and N-containing mesoporous carbon exhibit high selectivity to the target product, VDF. However, these catalysts are difficult to recover following deactivation.

During the pyrolysis of HCFC-142b, the following reactions take place. Dehydrochlorination (DeHCl) of HCFC-142b leads to the formation of VDF. However, dehydrofluorination (DeHF) and Cl/F exchange reactions produce vinylidene chlorofluoride (VCF), CH<sub>3</sub>CF<sub>3</sub>, and CH<sub>3</sub>CCl<sub>2</sub>F. Hence, the catalyst plays a major role in the selectivity.



Due to the formation of highly corrosive HCl and HF in the dehydrochlorination and dehydrofluorination reactions, the selection of catalyst is limited to corrosion resistant materials. Therefore, carbon materials [8,9], fluorinated Cr<sub>2</sub>O<sub>3</sub> [10–12], and metal fluorides [13–16] were suggested. Especially, metal fluorides have been evaluated as the catalysts for the pyrolysis of HCFC-142b [17]. It was found that BaF<sub>2</sub> shows high activity and selectivity to VDF. However, it deactivates rapidly due to the chlorination of BaF<sub>2</sub> to BaClF and BaCl<sub>2</sub> during reaction.

SrF<sub>2</sub> also exhibits high activity for the decomposition of HCFC-142b to VDF under mild conditions. However, the selectivity to the target product, VDF, is rather low [7]. Although the preparation of SrF<sub>2</sub> microparticles with cubic structures improves the performance, the procedure is complicated and difficult to scale up. It is well accepted that the metal–support interaction plays a major role in the selectivity of catalytic reaction [18–20]. Actually, the selectivity of catalysts is possible to be controlled by electronic charge of the metal because of the metal–support interaction. Electrons can transfer from the support to the metallic phases and change the metal–reactants interaction [21].

Although being N-doped carbon materials [5,6], BaF<sub>2</sub> and SrF<sub>2</sub> were suggested to be efficient catalysts for the pyrolysis of HCFC-142b [5,6]. However, the conversion, selectivity, and stability of catalysts are far from the industrial application at present. Hence, it necessitates the study of catalysts in depth. In this work, SrF<sub>2</sub>@C (SrF<sub>2</sub> embedded in carbon) and SrF<sub>2</sub>@NC (N-doped carbon) catalysts were fabricated following calcination in N<sub>2</sub> with SrC<sub>2</sub>O<sub>4</sub>, PVDF (and urea as the precursors). The effects of calcination temperatures and doping of N to carbon shell on the metal–support interaction as well as the selectivity of HCFC-142b pyrolysis were investigated systematically.

## 2. Results and Discussion

The catalysts obtained by mechanical milling and calcination (SrF<sub>2</sub>@C and SrF<sub>2</sub>@NC) as well as SrF<sub>2</sub> prepared by precipitation were evaluated as the catalysts for the pyrolysis of HCFC-142b. Compared with the industrial reaction [22], the presence of SrF<sub>2</sub> catalysts reduced the pyrolysis temperature from 650 °C to 350 °C (Figure 1a). In addition to the HCl and HF acids, the major carbon-containing products are vinyl difluoride (CH<sub>2</sub>=CF<sub>2</sub>, VDF) via dehydrochlorination (DeHCl) and vinyl chlorofluoride (CH<sub>2</sub>=ClF, VCF) via dehydrofluorination (DeHF). Minor products with trace amounts include CH<sub>3</sub>CF<sub>3</sub> and CH<sub>3</sub>CCl<sub>2</sub>F via F/Cl exchange reaction. Clearly, both DeHCl and DeHF reactions prevail over SrF<sub>2</sub> catalyst, as VDF and VCF (other byproducts were detected in trace amounts) are the major products (Figure 1b).

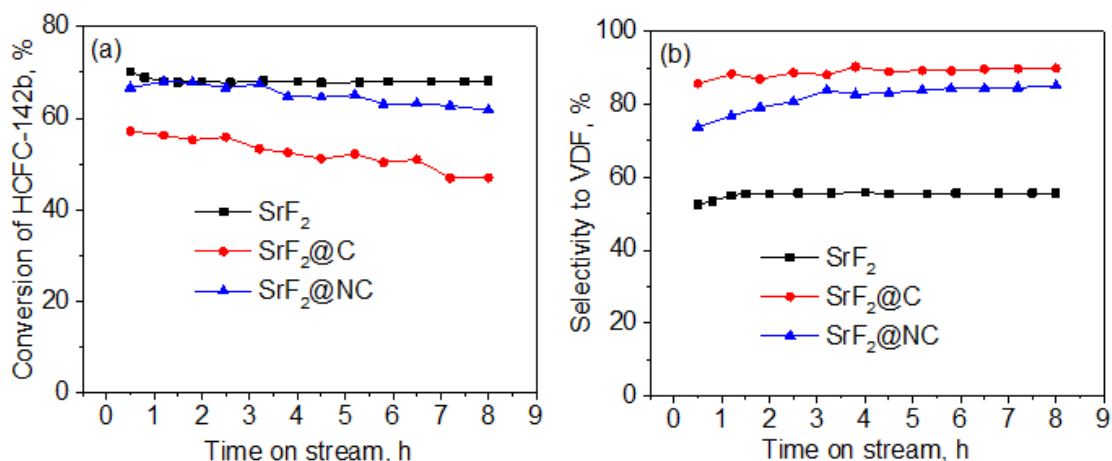


**Figure 1.** Catalytic performance of SrF<sub>2</sub> catalysts for the decomposition of HCFC-142b. (a) Conversion of HCFC-142b and (b) selectivity to vinylidene fluoride (VDF). Reactions were carried out at 350 °C, 1 bar, GHSV (HCFC-142b) of 600 h<sup>-1</sup> with N<sub>2</sub>:HCFC-142b of 1:1.

Following the preparation of SrF<sub>2</sub>@C catalyst, the conversion of HCFC-142b decreases significantly. This is attributed to the partial coverage of SrF<sub>2</sub> by carbon shell. Similar results have been reported in our previous work for MgF<sub>2</sub> catalysts embedded in carbon structures [23]. However, it is worth noting that the selectivity to VDF is increased from 50% to around 90%. Unexpectedly, the doping of N to carbon in SrF<sub>2</sub>@NC catalyst does not improve both the conversion and selectivity. As reported, N-doped carbon materials are effective catalysts for the dehydrochlorination of HCFC-142b at moderate temperatures [5,6]. We suggest that SrF<sub>2</sub> interacts with carbon in SrF<sub>2</sub>@C and SrF<sub>2</sub>@NC resulting in the change of conversion and selectivity. Another possibility is attributed to the insufficient calcination temperature. As mentioned in the Experimental section, both SrF<sub>2</sub>@C and SrF<sub>2</sub>@NC were prepared via calcination of SrC<sub>2</sub>O<sub>4</sub> and PVDF precursors at 390 °C. The calcination temperature is probably not high enough for the formation of SrF<sub>2</sub>@C and SrF<sub>2</sub>@NC catalysts.

Consequently, both the decomposition of SrC<sub>2</sub>O<sub>4</sub> and PVDF was investigated by TG and DTG techniques. The experiments were carried out under N<sub>2</sub> atmosphere in order to explore the precursor decomposition during the catalyst preparation process. As indicated in Figure 2a, the first step of SrC<sub>2</sub>O<sub>4</sub> decomposition was observed in the temperature range of 127–200 °C with a peak temperature of 110 °C. The weight loss of this step is 8.6%, which is equivalent to the loss of one water molecule (theoretical mass loss: 9.1%). Decomposition in the second step was observed in the temperature range of 400–600 °C, and the peak temperature was around 500 °C, which corresponds to the SrC<sub>2</sub>O<sub>4</sub> decomposition to SrCO<sub>3</sub> and CO (mass loss of 14.1%) [24–26]. Figure 2b discloses the decomposition of PVDF. The pyrolysis of PVDF commences at 390 °C, and two peak temperatures at about 455 °C and 465 °C are found. Clearly, calcination at 390 °C affords the decomposition of SrC<sub>2</sub>O<sub>4</sub> and PVDF [27]. However, calcination temperature plays a major role in the metal–support interaction [28]. Consequently, the SrF<sub>2</sub>@C catalysts were further calcined at elevated temperatures.

The catalytic activities for SrF<sub>2</sub>@C catalysts calcined at temperatures between 500 °C and 900 °C are displayed in Figure 3. The average conversion of HCFC-142b over SrF<sub>2</sub>@C obtained by the calcination at 390 °C is about 55%. With the increase in calcination temperature to 500 °C, the conversion of HCFC-142b drops dramatically to about 15%. Further increase the calcination temperature to 600 °C and 700 °C, and higher conversion levels of 62% and 75% than that at 390 °C are achieved. When the calcination temperature reaches 800 °C, the activity declines to 42% again. The highest selectivity to VDF is obtained over catalysts calcined at 390 °C and 500 °C with the average selectivity of 88% and 81%, respectively. However, it should be noted that the conversion is rather low on the catalyst calcined at 500 °C (12%). It seems that the catalyst calcined at 390 °C exhibits the best performance for the pyrolysis of HCFC-142b. Although the activities with the catalysts calcined at 600 °C and 700 °C

are relatively high, the selectivity to VDF is particularly poor, and the selectivity to VCF (via DeHF) can be as high as 90%. Clearly, both DeHCl (forming VDF) and DeHF (Forming VCF) reactions compete with each other over SrF<sub>2</sub>@C catalysts.

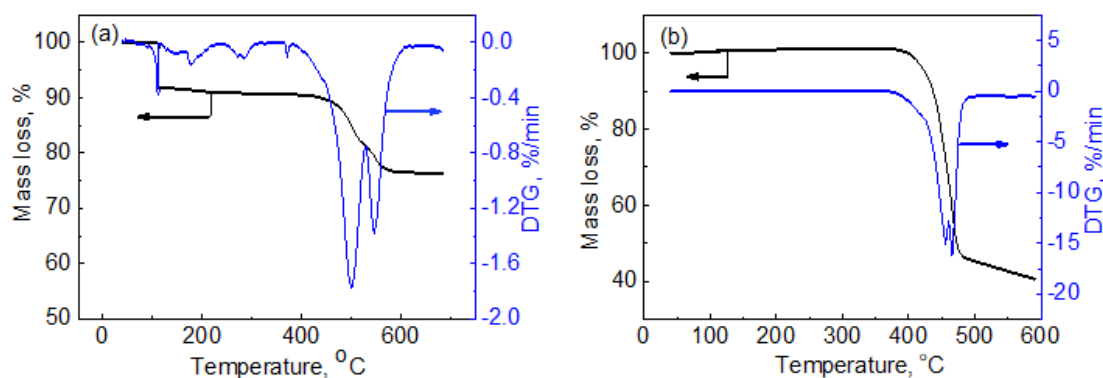


**Figure 2.** Thermogravimetry (TG) and DTG (derivative thermogravimetry) of SrC<sub>2</sub>O<sub>4</sub> (a) and PVDF (b). The ramp rate was set to 10 °C/min during the experiments.

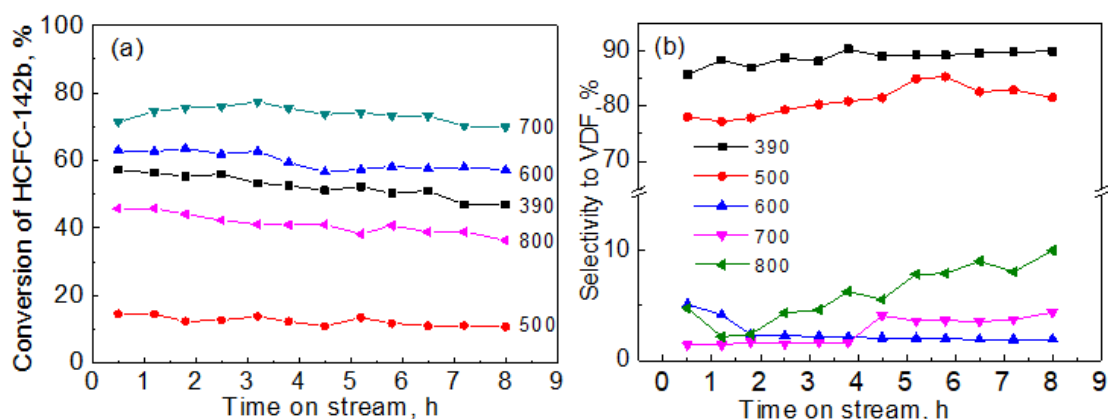


**Figure 3.** Effect of calcination temperature on the catalytic performance of SrF<sub>2</sub>@C catalysts for the decomposition of HCFC-142b. (a) Conversion of HCFC-142b and (b) selectivity to VDF. Reactions were carried out at 350 °C, 1 bar, GHSV (HCFC-142b) of 600 h<sup>-1</sup> with N<sub>2</sub>:HCFC-142b of 1:1.

Clearly, the variation of conversion and selectivity is not ascribed to the sintering of SrF<sub>2</sub> at elevated calcination temperatures. As presented in Figure 4, the XRD patterns of SrF<sub>2</sub>@C catalysts calcined at different temperatures were obtained. The diffraction peaks of SrF<sub>2</sub> in SrF<sub>2</sub>@C catalyst agree well with the standard XRD card of SrF<sub>2</sub> (PDF #88-2294 of The Joint Committee on Powder Diffraction Standards, JCPDS). No other impurities were detected. Even with the calcination of 390 °C, clean SrF<sub>2</sub> crystalline structures were achieved. It further confirms the decomposition of PVDF and fluorination of Sr species to SrF<sub>2</sub> during calcination with SrC<sub>2</sub>O<sub>4</sub> and PVDF as the precursors. Hence, the difference of catalytic performance over SrF<sub>2</sub>, SrF<sub>2</sub>@C, and SrF<sub>2</sub>@NC in Figure 1 cannot be attributed to the low calcination temperature (390 °C). Additionally, the change in conversion and selectivity in Figure 3 following elevated calcination temperatures is not resulted from the sintering of SrF<sub>2</sub>. All diffraction peaks in the figure are sharp, and the intensity is relatively high, indicating that the prepared catalysts are well crystallized. No other impurities were found in all the samples, suggesting that Sr is fully fluorinated to SrF<sub>2</sub>. With the increase in calcination temperature, the intensity of the diffraction peaks almost keeps unchanged. The crystalline sizes were further estimated by the Selyakov–Scherer equation. Following calcination at elevated temperatures, the crystalline slightly increased from 28 nm to 31 nm. Evidently, no significant sintering of SrF<sub>2</sub> is detected at elevated calcination temperatures.

Clearly, it suggests that embedding of SrF<sub>2</sub> particles in the carbon structure prevents the particles from sintering at high temperatures.

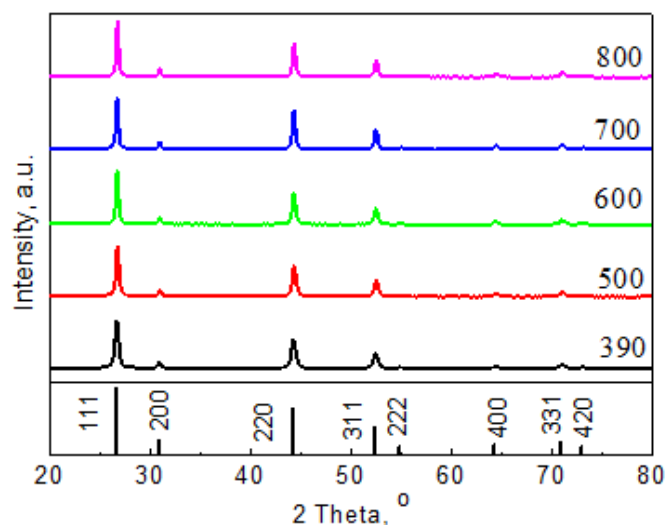


**Figure 4.** The X-ray patterns for SrF<sub>2</sub>@C catalysts with calcination at different temperatures and the standard profile of SrF<sub>2</sub> (PDF #88-2294).

In addition to the crystalline size, no significant change in morphology was observed following calcination at elevated temperatures (Figure S1). Similarly, no dramatic change in porous structures was found (Figure S2 and Table S1). It is worth noting that the specific surface area of the SrF<sub>2</sub>@C catalyst is much higher than that of the precipitated SrF<sub>2</sub> (15 m<sup>2</sup>/g). It also proves that mesoporous carbon structures in SrF<sub>2</sub>@C catalysts with surface areas of 156 m<sup>2</sup>/g to 257 m<sup>2</sup>/g afford the exposure of SrF<sub>2</sub>.

Therefore, the difference in Figures 1 and 3 can only be attributed to the change in the metal–support interaction. As confirmed in Figure S3, in the absence of carbon shell, no such significant change in HCFC-142b conversion and VDF selectivity are observed. For SrF<sub>2</sub> prepared by precipitation, only a slight decrease in conversion is detected following calcination at 700 °C. Furthermore, selectivity to VDF keeps almost unchanged. Clearly, metal–support interaction plays a critical role in the pyrolysis of HCFC-142b, especially the selectivity—namely, the competition of DeHCl and DeHF over SrF<sub>2</sub>.

Interestingly, in the presence of N element in carbon structure, conversion of HCFC-142b decreases significantly following calcination at 700 °C (Figure 5a). More importantly, VCF (via DeHF reaction) is the major product for SrF<sub>2</sub>@C-700 catalyst (Figure 5b). With the doping of N, the selectivity to VDF (via DeHCl reaction) is higher than 85% with selectivity to VCF lower than 15%. Clearly, simple doping of N switches the major product from VCF to VDF, or the reaction from DeHF to DeHCl. The addition of urea during catalyst preparation changed the properties of the catalyst.

However, modification of N-doping amounts does not affect the selectivity of HCFC-142b decomposition (Figure S4). The dramatic change in conversion can be explained by the change in pore structure and surface area (Figure S5 and Table S2). With high N-doping amounts, both mesoporous structure and surface area decrease result in the decline of conversion level. The morphology disclosed by SEM reinforces the above results. With high loading of N, relatively large particles are resulted (Figure S6).

As discussed previously, the change in support property leads to the variation of metal–support interaction significantly. Consequently, both the conversion and selectivity are changed accordingly. To elucidate this argument, additional characterization experiments were conducted.

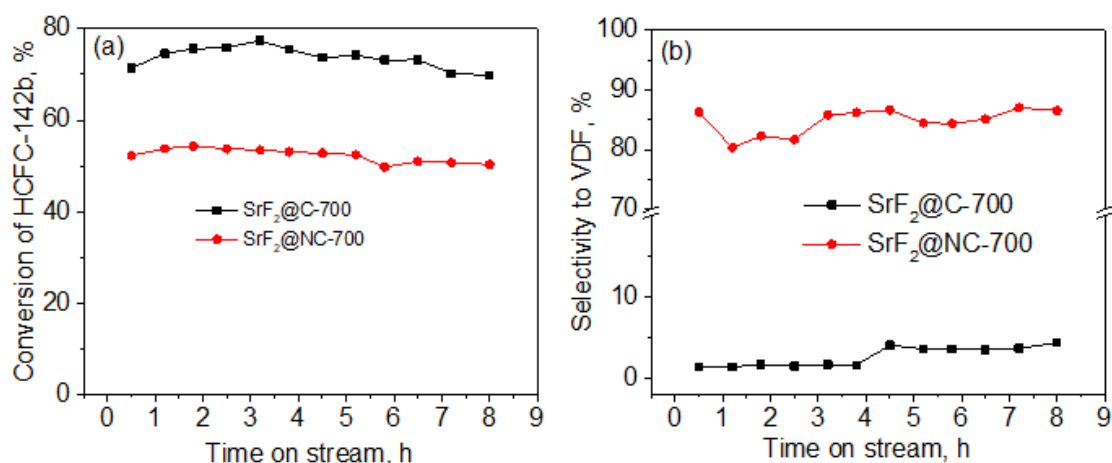


**Figure 5.** Catalytic performance of SrF<sub>2</sub>@C and SrF<sub>2</sub>@NC catalysts calcined at 700 °C for the decomposition of HCFC-142b. (a) Conversion of HCFC-142b and (b) selectivity to VDF. Reactions were carried out at 350 °C, 1 bar, GHSV (HCFC-142b) of 600 h<sup>-1</sup> with N<sub>2</sub>:HCFC-142b of 1:1.

The morphology of SrF<sub>2</sub>@C, SrF<sub>2</sub>@NC, SrF<sub>2</sub>@C-700, and SrF<sub>2</sub>@NC-700 was first investigated by SEM (Figure 6). For SrF<sub>2</sub>@C and SrF<sub>2</sub>@NC catalysts, small and sheetlike structure is obtained. Following calcination of 700 °C, larger and solid particles are achieved. Although the mesoporous carbon facilitates the exposure, calcination at high temperature clearly leads to the decrease in surface area. Consequently, decreased conversion of HCFC-142b was detected. As confined in the carbon structure, no noticeable sintering of SrF<sub>2</sub> was found (Figure 4). The conversion decrease (Figure 5a), which resulted from catalyst calcination at 700 °C, is attributed to the loss of porosity by calcination at 700 °C.

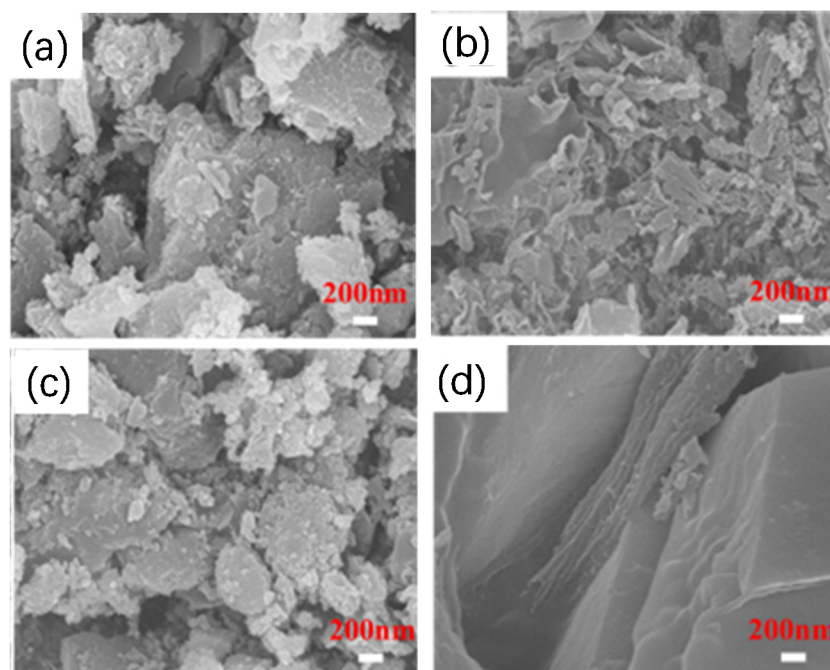


**Figure 6.** SEM images of (a) SrF<sub>2</sub>@C, (b) SrF<sub>2</sub>@NC, (c) SrF<sub>2</sub>@C-700, and (d) SrF<sub>2</sub>@NC-700.

The catalysts were further examined by TEM (Figure 7). As highlighted by the inset of Figure 7a,d, SrF<sub>2</sub> particles are clearly embedded in the carbon structure, and the particles are separated from each other by the carbon structure. Even with calcination at 700 °C, ultrafine particles are retained. The selected area electron diffraction (SAED) reinforces that the SrF<sub>2</sub> particles are highly crystallized (white spot). However, the SAED does not form a completed diffraction ring, which is a structure in which the particles are separated by carbon-containing compounds [29,30]. Consistent with XRD patterns, the most developed (111) facet is observed in the high-resolution TEM images with the fringe space of 0.35 nm both for SrF<sub>2</sub>@C and SrF<sub>2</sub>@NC-700 catalysts (Figure S7). It is noted that high-temperature calcination plays a role in the structure of carbon shell. As demonstrated in Figure 7a,b, without calcination at 700 °C, amorphous carbon structure is achieved. Following calcination, graphite sheetlike structure is obtained (Figure 7c,d). Clearly, carbon materials derived from the decomposition of PVDF underwent partial graphitization [31,32].

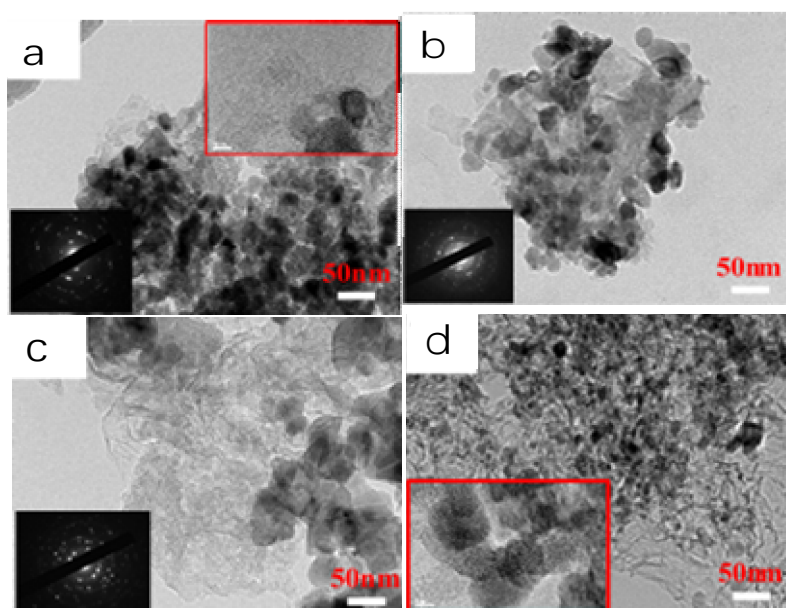


**Figure 7.** TEM images of (a) SrF<sub>2</sub>@C, (b) SrF<sub>2</sub>@NC, (c) SrF<sub>2</sub>@C-700, and (d) SrF<sub>2</sub>@NC-700.

Different from carbon shell, the doping of N and calcination at 700 °C did not change the crystalline structure of SrF<sub>2</sub>. As demonstrated in Figure 8, almost identical XRD patterns were obtained for SrF<sub>2</sub>@C, SrF<sub>2</sub>@NC, SrF<sub>2</sub>@C-700, and SrF<sub>2</sub>@NC-700. Based on the XRD patterns, the crystalline sizes are all around 28 nm to 31 nm. Similar with the results in Figure 4, the dramatic change of selectivity for the catalytic pyrolysis of HCFC-142b is not caused by the crystalline structure of SrF<sub>2</sub>. As exhibited in Figure S7, (111) facet allows major exposure for both catalysts.

Figure 9 displays the N<sub>2</sub> adsorption–desorption isotherm of SrF<sub>2</sub>@C, SrF<sub>2</sub>@C-700, SrF<sub>2</sub>@NC, and SrF<sub>2</sub>@NC-700. Clearly, the adsorption isotherms of all these samples exhibit type IV characteristics (classified by IUPAC) [33]. The clear capillary condensation process and H3-type hysteresis loops represent typical porous carbon materials. As listed in Table S3, the specific surface area of the SrF<sub>2</sub>@NC catalyst calcined at 700 °C is smaller than the specific surface area of the SrF<sub>2</sub>@NC catalyst (97 m<sup>2</sup>/g vs. 325 m<sup>2</sup>/g). It is ascribed to the urea decomposition and polycondensation leading to the blocking of the pore. It explains that conversion of HCFC-142b drops significantly following N-doping in Figure 5.

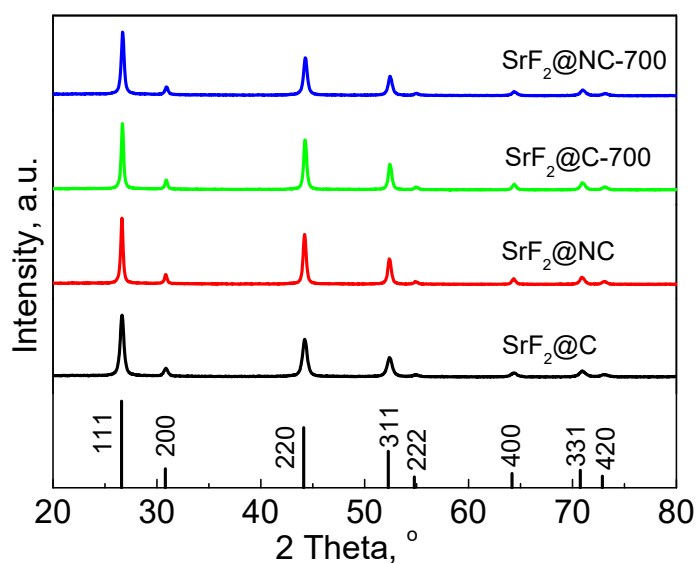


**Figure 8.** The X-ray diffractograms for SrF<sub>2</sub> catalysts and the standard profile of SrF<sub>2</sub> (PDF #88-2294).

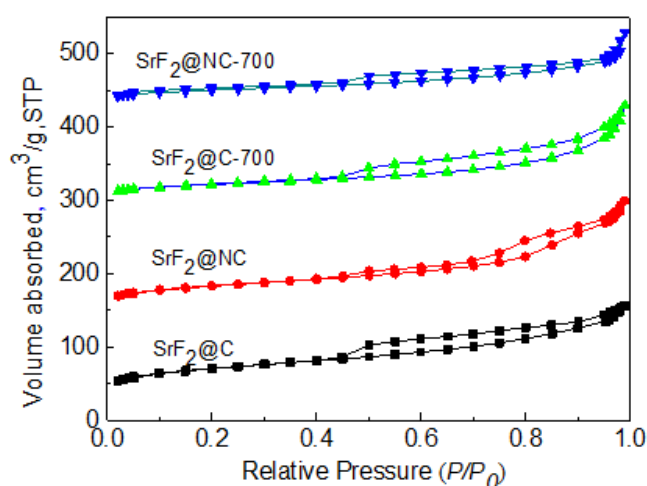


**Figure 9.** N<sub>2</sub> adsorption-desorption isotherms of SrF<sub>2</sub>@C, SrF<sub>2</sub>@C-700, SrF<sub>2</sub>@NC, and SrF<sub>2</sub>@NC-700.

The surface chemistry was explored by XPS for SrF<sub>2</sub>@C, SrF<sub>2</sub>@C-700, SrF<sub>2</sub>@NC, and SrF<sub>2</sub>@NC-700 catalysts. As revealed in Figure 10, SrF<sub>2</sub>@C and SrF<sub>2</sub>@C-700 mainly contain F, C, and Sr. N is identified over SrF<sub>2</sub>@NC and SrF<sub>2</sub>@NC-700. The surface element contents of these catalysts determined by XPS are listed in Table S4. It can be seen from the table that the contents of nitrogen are as high as 6% and 7% over SrF<sub>2</sub>@NC and SrF<sub>2</sub>@NC-700 catalysts, respectively, which indicates that N has been successfully doped to the catalysts by simple mixing with urea and calcination. In addition, F/Sr molar ratio in Table S4 for all the samples is higher than 2. We suggest that small amounts of F still remain in the carbon structures.

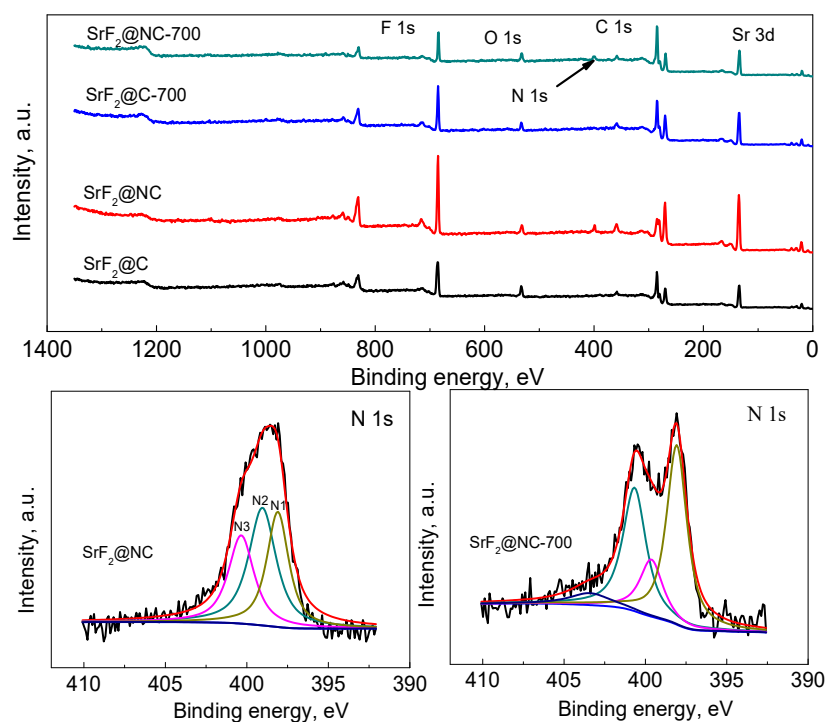


**Figure 10.** XPS spectra of SrF<sub>2</sub>@C, SrF<sub>2</sub>@C-700, SrF<sub>2</sub>@NC, and SrF<sub>2</sub>@NC-700 catalysts.

With the deconvolution of high-resolution N 1s spectra (Figure 10), four peaks correspond to four different N species—pyridine nitrogen ( $\approx 398.5$  eV, N1), pyrrole nitrogen ( $\approx 400.1$  eV, N2), graphite nitrogen ( $\approx 401.2$  eV, N3), and oxidized nitrogen ( $\approx 405.0$  eV, N4) are identified, respectively [34,35]. From the N 1s peak, it can be seen that there is less graphite nitrogen in SrF<sub>2</sub>@NC catalyst. With the calcination temperature of 700 °C, the proportion of graphite nitrogen increases and the proportion of pyrrole nitrogen decreases. It is consistent with reports that pyrrole nitrogen tends to transform to pyridine nitrogen at high temperatures and pyridine nitrogen can convert to graphitic nitrogen [36,37].

The high-resolution XPS spectra of Sr 3d and F 1s are shown in Figure 11. For SrF<sub>2</sub>@C and SrF<sub>2</sub>@NC catalysts, the binding energy of Sr 3d<sub>5/2</sub> is 134 eV, which agrees well with the Sr in SrF<sub>2</sub> [38,39]. With SrF<sub>2</sub>@C calcined at 700 °C, binding energy of Sr 3d<sub>5/2</sub> shifts to 134.5 eV. Clearly, calcination enhances the interaction between Sr and carbon shell. The shift towards higher binding energy indicates that carbon support withdraws electrons from Sr. As a result, the selectivity to VDF decreases significantly. With high electron deficiency, Sr tends to adsorb F with higher electronegativity. Thus, DeHF is facilitated, leading to the formation of VCF.

By contrast, the binding energy of Sr for SrF<sub>2</sub>@NC catalyst shifts to a lower position following calcination. With the transformation of pyrrole nitrogen to pyridine nitrogen and pyridine nitrogen to graphitic nitrogen at high temperatures, the interaction of Sr with N-doped carbon supplies electrons from N species. We suggest that N as an electron donor combines with Sr and supplies electrons. Consequently, DeHCl is enhanced and VDF prevails as the product. Similar shift trends are also identified for F 1s peaks. It further reinforces the effect of metal–support interaction on the selectivity of reactions. Therefore, the electron supply from N caused a change in the surface chemistry of the catalyst calcined at 700 °C. This change can be adopted to explain the selective dehydrochlorination and selective dehydrofluorination over SrF<sub>2</sub>@NC-700 and SrF<sub>2</sub>@C-700 catalysts in Figure 5.

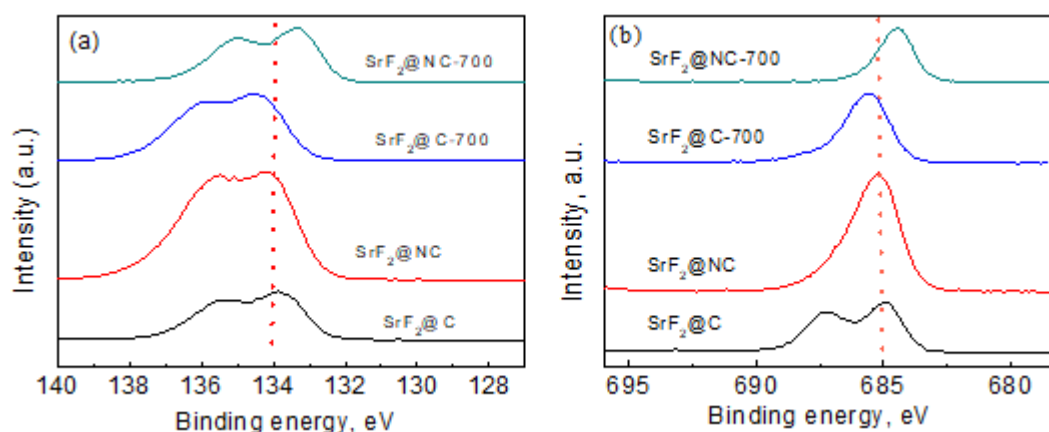


**Figure 11.** High-resolution XPS spectra of (a) Sr 3d and (b) F 1s for SrF<sub>2</sub>@C, SrF<sub>2</sub>@C-700, SrF<sub>2</sub>@NC, and SrF<sub>2</sub>@NC-700 catalysts.

### 3. Materials and Methods

#### 3.1. Catalyst Preparation

##### 3.1.1. Preparation of SrF<sub>2</sub> Embedded in Carbon Catalyst

Firstly, SrC<sub>2</sub>O<sub>4</sub> was prepared as follows: 0.1 mol of SrCl<sub>2</sub>·6H<sub>2</sub>O (99.5%, Aladdin Co., Shanghai, China) was stirred and dissolved in 200 mL of deionized water, and then H<sub>2</sub>C<sub>2</sub>O<sub>4</sub> was added according to the stoichiometric ratio. Following stirring for 2 h, it was filtered and washed to obtain a white paste. The paste was dried in an oven at 110 °C for 12 h to obtain SrC<sub>2</sub>O<sub>4</sub> precursor.

Desired amounts of SrC<sub>2</sub>O<sub>4</sub> and PVDF (poly-vinylidene fluoride, HSV900, average molecular weight of 1,100,000 g mol<sup>-1</sup>, Arkema Co., France) were added to the grinding mortar with a mass ratio of 1: 2. Following being fully ground uniformly, the mixture was placed in a tube furnace and calcined in N<sub>2</sub> atmosphere at a temperature of 390 °C for 5 h. During calcination, PVDF decomposed into carbon materials after release of HF [40,41]. As a result, Sr species were fluorinated to SrF<sub>2</sub> simultaneously. The catalyst is denoted as SrF<sub>2</sub>@C. To enhance the interaction between Sr and carbon, the catalysts were further calcined at temperatures between 500 °C and 800 °C in N<sub>2</sub> atmosphere and the catalyst was marked as SrF<sub>2</sub>@C-T, where T indicates the calcination temperature.

##### 3.1.2. Preparation of SrF<sub>2</sub> Embedded in N-Doped Carbon Catalyst

The preparation steps of the catalysts are the same as those of the SrF<sub>2</sub>@C catalyst, except that different proportions of urea are added as a nitrogen source during the grinding process. The catalysts are marked as SrF<sub>2</sub>@NC catalysts. For the catalysts which were calcined at temperatures between 500 °C and 800 °C in N<sub>2</sub> atmosphere, they are named as SrF<sub>2</sub>@NC-T, where T indicates the calcination temperature.

##### 3.1.3. Preparation of SrF<sub>2</sub> Catalyst

As comparison, SrF<sub>2</sub> was also synthesized by precipitation according to our previous study [7]. Prior to preparation, 2.3 g (0.1 mol) SrCl<sub>2</sub>·6H<sub>2</sub>O was dissolved in 200 mL deionized water. Equimolar NH<sub>4</sub>F was added stepwise. Following vigorous stirring for 2 h, the solution was filtered using a Buchner funnel with a vacuum pump. The paste was dried at 80 °C for 12 h. The sample is denoted as SrF<sub>2</sub>.

### 3.2. Catalyst Characterization

The surface areas of all the catalysts were measured by N<sub>2</sub> adsorption–desorption at −196 °C over Autosorb-1/C gas sorption analyzer (Quantachrome Instruments, Florida, USA). Prior to the measurement, the catalysts were evacuated at 200 °C for 5 h. The surface area was calculated according to the Brunauer–Emmett–Teller (BET) equation. Scanning electron microscope (SEM) was adopted for the investigation of morphology. SEM images were taken from Hitachi S-4700(II) (Hitachi, Japan). The operating voltage was set to be 15 kV. The samples were gold-sputtering-treated for better resolution of SEM images. High-resolution transmission electron microscope (TEM) was used for the elucidation of microstructures of catalysts. TEM images were obtained from a JEM-1200EX microscope (JEOL, Japan) at 200 kV. Thermogravimetry (TG/DTG) experiments were conducted over NETZSCH-STA449C with ramp rate of 10 °C/min in N<sub>2</sub> atmosphere. The crystalline structure was analyzed by X-ray diffraction (XRD) over X, Pert Pro (PANalytical, Netherlands) with Cu K $\alpha$  radiation source ( $\lambda = 1.5406$ ). The operating voltage was maintained at 40 kV and a current of 30 mA. The surface chemistry of catalysts was studied by X-ray photoelectron spectroscopy (XPS) on ESCALAB 250XI with Al K $\alpha$  as the radiation source (24.2 W).

### 3.3. Catalytic Tests

The activity of catalysts was evaluated by a fixed bed reactor (Ni tube with the purity of  $\geq 99.6\%$ ). The inner diameter of the reactor is 12 mm with a thickness of 4 mm. The isothermal zone of the reactor was determined to be 50 mm. The feed gas, HCFC-142b, diluted by equimolar amounts of N<sub>2</sub> was controlled by mass flow rate controllers (D07, Seven star, Beijing, China). Reactions were carried out at 350 °C, 1 bar, GHSV (HCFC-142b) of 600 h<sup>−1</sup>. Following reactions, the product stream was scrubbed by KOH solution (450 mL) for the removal of acid gases including HCl and HF. The composition of products was determined by gas chromatography (GC-1690, JieDao, Hangzhou, China) with a thermal conductivity detector (TCD). During the analysis, the products were separated by 5% ODPN (oxydipropionitrile) in the analytical column of the gas chromatography.

## 4. Conclusions

SrF<sub>2</sub> is the effective catalyst for the pyrolysis of HCFC-142b, which reduces the reaction temperature from 650 °C–700 °C to 350 °C. However, the selectivity to target product, VDF, is rather low. In the present work, SrF<sub>2</sub>@C catalysts were successfully prepared with SrC<sub>2</sub>O<sub>4</sub> and PVDF as the precursors following calcination in N<sub>2</sub> atmosphere. During calcination, the addition of urea led to the formation of SrF<sub>2</sub>@NC (N-doped carbon). For the pyrolysis of HCFC-142b, the dehydrochlorination (DeHCl) forms VDF and while dehydrofluorination (DeHF) produces VCF. Both DeHCl and DeHF compete with each other over SrF<sub>2</sub>. Both the calcination temperature and N-doping play a role in the conversion and selectivity of HCFC-142b. Calcination at elevated temperatures enhances the Sr-C interaction. For SrF<sub>2</sub>@C, improved interaction facilitates withdrawing electron from Sr by the carbon support. By contrast, the strong interaction of Sr with N-doped carbon supplies electrons from N species to Sr. The electron deficiency of Sr is favorable for the adsorption of F with higher electronegativity and consequently DeHF reaction forming VCF. The supply of electrons to Sr by the support improves the formation of VDF (DeHCl).

**Supplementary Materials:** The following are available online at <http://www.mdpi.com/2073-4344/10/3/355/s1>, Figure S1: SEM images of SrF<sub>2</sub>@C catalysts calcined at different temperatures. (a) SrF<sub>2</sub>@C (390), (b) SrF<sub>2</sub>@C-500, (c) SrF<sub>2</sub>@C-600, (d) SrF<sub>2</sub>@C-700, (e) SrF<sub>2</sub>@C-800. Figure S2: N<sub>2</sub> adsorption–desorption isotherms of SrF<sub>2</sub>@C. Figure S3: catalytic performance of SrF<sub>2</sub> prepared by precipitation and calcined at 700 °C for the decomposition of HCFC-142b. Figure S4: catalytic performance of SrF<sub>2</sub>@CN with different doping amount of urea for the decomposition of HCFC-142b. Figure S5: N<sub>2</sub> adsorption–desorption isotherms of SrF<sub>2</sub>@NC with different doping amounts of urea during catalyst preparation. Figure S6: SEM images of SrF<sub>2</sub>@NC catalysts prepared by doping different amounts of urea during catalyst preparation. Figure S7s: high-resolution TEM images of SrF<sub>2</sub>@C and SrF<sub>2</sub>@NC-700 catalysts. Table S1: textural parameters of SrF<sub>2</sub>@C samples. Table S2: structural parameters of SrF<sub>2</sub>@NC catalyst prepared with different doping amounts of urea. Table S3: textural parameters of SrF<sub>2</sub>@C,

SrF<sub>2</sub>@NC, SrF<sub>2</sub>@C-700, and SrF<sub>2</sub>@NC-700. Table S4: surface element content of SrF<sub>2</sub>@C, SrF<sub>2</sub>@NC, SrF<sub>2</sub>@C-700, and SrF<sub>2</sub>@NC-700 catalysts determined by XPS.

**Author Contributions:** W.H. and W.L. conceived and designed the experiments; Y.L. and Z.W. performed the experiments; W.H. and W.L. analyzed the data; K.M.M., S.W., and W.Y. characterized the catalysts; W.L., J.Z., and S.W. contributed reagents/materials/analysis tools; W.H. and Z.W. wrote the paper. W.L. and K.M.M. revised the paper. All authors have read and agreed to the published version of the manuscript.

**Funding:** This research was supported by National Key Research and Development Project of China (2019YFC0214504), Zhejiang Provincial Natural Science Foundation of China under grant no. LY19B060009 and Key Research and Development Project of Zhejiang Province (2020C01120).

**Conflicts of Interest:** The authors declare no conflict of interest. The founding sponsors had no role in the design of the study; in the collection, analyses, or interpretation of data; in the writing of the manuscript, or in the decision to publish the results.

## References

1. Ameduri, B. From Vinylidene Fluoride (VDF) to the Applications of VDF-Containing Polymers and Copolymers: Recent Developments and Future Trends. *Chem. Rev.* **2009**, *109*, 6632–6686. [[CrossRef](#)]
2. Taguet, A.; Ameduri, B.; Boutevin, B. Crosslinking of vinylidene fluoride-containing fluoropolymers. In *Crosslinking in Materials Science*; Ameduri, B., Ed.; Springer: Berlin/Heidelberg, Germany, 2005; Volume 184, pp. 127–211.
3. Wang, L.; Liu, S.; He, H.Q.; Zhang, J.L. Dual-level direct dynamics study on the hydrogen abstraction reaction of fluorine atom with 1,1-difluoro-1-chloroethane. *Can. J. Chem.-Revue Canadienne De Chimie* **2011**, *89*, 1396–1402. [[CrossRef](#)]
4. Huybrechts, G.; Van Assche, G.; Van der Auwera, S. Kinetics and mechanism of the pyrolysis of 1-chloro-1,1-difluoroethane in the presence of additives. *Int. J. Chem. Kinet.* **1998**, *30*, 359–366. [[CrossRef](#)]
5. Wang, Z.; Han, W.; Zhang, C.; Zhou, S.; Wang, H.; Tang, H.; Liu, H. Preparation of N-Doped Activated Carbon for Catalytic Pyrolysis of 1-Chloro-1,1-difluoroethane to Vinylidene Fluoride. *Chemistryselect* **2018**, *3*, 1015–1018. [[CrossRef](#)]
6. Wang, Z.; Han, W.; Tang, H.; Li, Y.; Liu, H. Preparation of N-doped ordered mesoporous carbon and catalytic performance for the pyrolysis of 1-chloro-1,1-difluoroethane to vinylidene fluoride. *Microporous Mesoporous Mater.* **2019**, *275*, 200–206. [[CrossRef](#)]
7. Wang, Z.; Han, W.; Liu, H. EDTA-assisted hydrothermal synthesis of cubic SrF<sub>2</sub> particles and their catalytic performance for the pyrolysis of 1-chloro-1,1-difluoroethane to vinylidene fluoride. *Crystengcomm* **2019**, *21*, 1691–1700. [[CrossRef](#)]
8. Lan, G.J.; Wang, Y.; Qiu, Y.Y.; Wang, X.L.; Liang, J.; Han, W.F.; Tang, H.D.; Liu, H.Z.; Liu, J.; Li, Y. Wheat flour-derived N-doped mesoporous carbon extrudate as superior metal-free catalysts for acetylene hydrochlorination. *Chem. Commun.* **2018**, *54*, 623–626. [[CrossRef](#)] [[PubMed](#)]
9. Sun, X.; Liu, X.; Qin, Y.C.; Qiang, L.; He, Y.P.; Su, D.S.; Song, L.J.; Sun, Z.L. Direct Conversion of Acetylene and 1,2-Dichloroethane to Vinyl Chloride Monomer over a Supported Carbon Nitride Catalyst: Tunable Activity Controlled by the Synthesis Temperature. *Ind. Eng. Chem. Res.* **2019**, *58*, 5404–5413. [[CrossRef](#)]
10. Liu, B.; Han, W.F.; Li, X.L.; Li, L.C.; Tang, H.D.; Lu, C.S.; Li, Y.; Li, X.N. Quasi metal organic framework with highly concentrated Cr<sub>2</sub>O<sub>3</sub> molecular clusters as the efficient catalyst for dehydrofluorination of 1,1,1,3,3-pentafluoropropane. *Appl. Catal. B-Environ.* **2019**, *257*, 117939. [[CrossRef](#)]
11. Wang, H.L.; Han, W.F.; Li, X.L.; Liu, B.; Tang, H.D.; Li, Y. Solution Combustion Synthesis of Cr<sub>2</sub>O<sub>3</sub> Nanoparticles and the Catalytic Performance for Dehydrofluorination of 1,1,1,3,3-Pentafluoropropane to 1,3,3,3-Tetrafluoropropene. *Molecules* **2019**, *24*, 361. [[CrossRef](#)]
12. Han, W.F.; Wang, Z.K.; Li, X.J.; Tang, H.D.; Xi, M.; Li, Y.; Liu, H.Z. Solution combustion synthesis of nano-chromia as catalyst for the dehydrofluorination of 1,1-difluoroethane. *J. Mater. Sci.* **2016**, *51*, 11002–11013. [[CrossRef](#)]
13. Han, W.F.; Wang, J.C.; Chen, L.L.; Yang, L.T.; Wang, S.C.; Xi, M.; Tang, H.D.; Liu, W.C.; Song, W.Y.; Zhang, J.J.; et al. Reverting fluoroform back to chlorodifluoromethane and dichlorofluoromethane: Intermolecular Cl/F exchange with chloroform at moderate temperatures. *Chem. Eng. J.* **2019**, *355*, 594–601. [[CrossRef](#)]

14. Han, W.F.; Liu, B.; Li, X.L.; Yang, L.T.; Wang, J.C.; Tang, H.D.; Liu, W.C. Combustion Synthesis of Amorphous Al and Cr Composite as the Catalyst for Dehydrofluorination of 1,1-Difluoroethane. *Ind. Eng. Chem. Res.* **2018**, *57*, 12774–12783. [[CrossRef](#)]
15. Fang, X.X.; Liao, W.M.; Song, J.D.; Jia, W.Z.; Wang, Y.; Lu, J.Q.; Luo, M.F. Effect of Fe promotion on the performance of V<sub>2</sub>O<sub>5</sub>/MgF<sub>2</sub> catalysts for gas-phase dehydrofluorination of 1,1,1,3,3-pentafluoropropane. *Appl. Surf. Sci.* **2019**, *490*, 365–371. [[CrossRef](#)]
16. Mao, W.; Jia, Z.H.; Bai, Y.B.; Qin, Y.; Wang, B.; Han, S.; Zhang, W.; Kou, L.G.; Lu, J.; Kemnitz, E. Fe/hollow nano-MgF<sub>2</sub>: A green and highly-efficient alternative to classical Cr-based catalysts for the gas-phase fluorination reaction. *Catal. Sci. Technol.* **2019**, *9*, 3015–3019. [[CrossRef](#)]
17. Han, W.F.; Liu, B.; Kang, Y.K.; Wang, Z.K.; Yu, W.; Yang, H.; Liu, Y.N.; Lu, J.Q.; Tang, H.D.; Li, Y.; et al. Experimental and DFT Mechanistic Study of Dehydrohalogenation of 1-Chloro-1,1-difluoroethane over Metal Fluorides. *Ind. Eng. Chem. Res.* **2019**, *58*, 18149–18159. [[CrossRef](#)]
18. Oh, S.; Kim, Y.K.; Jung, C.H.; Doh, W.H.; Park, J.Y. Effect of the metal-support interaction on the activity and selectivity of methanol oxidation over Au supported on mesoporous oxides. *Chem. Commun.* **2018**, *54*, 8174–8177. [[CrossRef](#)]
19. Da Silva, A.B.; Jordao, E.; Mendes, M.J.; Fouilloux, P. Effect of metal-support interaction during selective hydrogenation of cinnamaldehyde to cinnamyl alcohol on platinum based bimetallic catalysts. *Appl. Catal. A-Gen.* **1997**, *148*, 253–264. [[CrossRef](#)]
20. Jenness, G.R.; Schmidt, J.R. Unraveling the Role of Metal-Support Interactions in Heterogeneous Catalysis: Oxygenate Selectivity in Fischer-Tropsch Synthesis. *ACS Catal.* **2013**, *3*, 2881–2890. [[CrossRef](#)]
21. Gross, E.; Somorjai, G.A. The Impact of Electronic Charge on Catalytic Reactivity and Selectivity of Metal-Oxide Supported Metallic Nanoparticles. *Top. Catal.* **2013**, *56*, 1049–1058. [[CrossRef](#)]
22. Wang, Z.K.; Han, W.F.; Tang, H.D.; Liu, H.Z. CaBaF<sub>x</sub> composite as robust catalyst for the pyrolysis of 1-chloro-1,1-difluoroethane to vinylidene fluoride. *Catal. Commun.* **2019**, *120*, 42–45. [[CrossRef](#)]
23. Han, W.F.; Zhang, C.P.; Wang, H.L.; Zhou, S.L.; Tang, H.D.; Yang, L.T.; Wang, Z.K. Sub-nano MgF<sub>2</sub> embedded in carbon nanofibers and electrospun MgF<sub>2</sub> nanofibers by one-step electrospinning as highly efficient catalysts for 1,1,1-trifluoroethane dehydrofluorination. *Catal. Sci. Technol.* **2017**, *7*, 6000–6012. [[CrossRef](#)]
24. Al-Newaiser, F.A.; Al-Thabaiti, S.A.; Al-Youbi, A.O.; Obaid, A.Y.; Gabal, M.A. Thermal decomposition kinetics of strontium oxalate. *Chem. Pap.* **2007**, *61*, 370–375. [[CrossRef](#)]
25. Dollimore, D.; Heal, G.R.; Passalis, N.P. The thermal analysis of strontium oxalate. *Thermochim. Acta* **1985**, *92*, 543–546. [[CrossRef](#)]
26. Nagase, K.; Sato, K.; Tanaka, N. Thermal Dehydration and Decomposition Reactions of Bivalent Metal Oxalates in the Solid State. *Bull. Chem. Soc. Jpn.* **1975**, *48*, 439–442. [[CrossRef](#)]
27. Han, W.F.; Wang, H.L.; Liu, B.; Li, X.L.; Tang, H.D.; Li, Y.; Liu, H.Z. PVDF mediated fabrication of freestanding AlF<sub>3</sub> sub-microspheres: Facile and controllable synthesis of alpha, beta and theta-AlF<sub>3</sub>. *Mater. Chem. Phys.* **2020**, *240*, 122287. [[CrossRef](#)]
28. Song, S.H.; Son, J.H.; Budiman, A.W.; Choi, M.J.; Chang, T.S.; Shin, C.H. The influence of calcination temperature on catalytic activities in a Co based catalyst for CO<sub>2</sub> dry reforming. *Korean J. Chem. Eng.* **2014**, *31*, 224–229. [[CrossRef](#)]
29. Harris, L.A.; Goff, J.D.; Carmichael, A.Y.; Riffle, J.S.; Harburn, J.J.; St Pierre, T.G.; Saunders, M. Magnetite nanoparticle dispersions stabilized with triblock copolymers. *Chem. Mater.* **2003**, *15*, 1367–1377. [[CrossRef](#)]
30. Yang, X.N.; van Duren, J.K.J.; Janssen, R.A.J.; Michels, M.A.J.; Loos, J. Morphology and thermal stability of the active layer in poly(p-phenylenevinylene)/methanofullerene plastic photovoltaic devices. *Macromolecules* **2004**, *37*, 2151–2158. [[CrossRef](#)]
31. Hou, J.; Cao, C.; Idrees, F.; Ma, X. Hierarchical Porous Nitrogen-Doped Carbon Nanosheets Derived from Silk for Ultrahigh-Capacity Battery Anodes and Supercapacitors. *ACS Nano* **2015**, *9*, 2556–2564. [[CrossRef](#)] [[PubMed](#)]
32. Rahaman, M.S.A.; Ismail, A.F.; Mustafa, A. A review of heat treatment on polyacrylonitrile fiber. *Polym. Degrad. Stab.* **2007**, *92*, 1421–1432. [[CrossRef](#)]
33. Thommes, M.; Kaneko, K.; Neimark, A.V.; Olivier, J.P.; Rodriguez-Reinoso, F.; Rouquerol, J.; Sing, K.S.W. Physisorption of gases, with special reference to the evaluation of surface area and pore size distribution (IUPAC Technical Report). *Pure Appl. Chem.* **2015**, *87*, 1051–1069. [[CrossRef](#)]

34. Hulicova-Jurcakova, D.; Kodama, M.; Shiraishi, S.; Hatori, H.; Zhu, Z.H.; Lu, G.Q. Nitrogen-Enriched Nonporous Carbon Electrodes with Extraordinary Supercapacitance. *Adv. Funct. Mater.* **2009**, *19*, 1800–1809. [[CrossRef](#)]
35. Ortega, K.F.; Arrigo, R.; Frank, B.; Schlogl, R.; Trunschke, A. Acid-Base Properties of N-Doped Carbon Nanotubes: A Combined Temperature-Programmed Desorption, X-ray Photoelectron Spectroscopy, and 2-Propanol Reaction Investigation. *Chem. Mater.* **2016**, *28*, 6826–6839. [[CrossRef](#)]
36. Arrigo, R.; Havecker, M.; Schlogl, R.; Su, D.S. Dynamic surface rearrangement and thermal stability of nitrogen functional groups on carbon nanotubes. *Chem. Commun.* **2008**, 4891–4893. [[CrossRef](#)]
37. Guo, L.S.; Zhang, P.P.; Cui, Y.; Liu, G.B.; Wu, J.H.; Yang, G.H.; Yoneyama, Y.; Tsubaki, N. One-Pot Hydrothermal Synthesis of Nitrogen Functionalized Carbonaceous Material Catalysts with Embedded Iron Nanoparticles for CO<sub>2</sub> Hydrogenation. *ACS Sustain. Chem. Eng.* **2019**, *7*, 8331–8339. [[CrossRef](#)]
38. Olive, G. (Ca, Sr)F<sub>2</sub> surface-roughness effect on angle-resolved xps measurements. *Surf. Sci.* **1993**, *297*, 83–90. [[CrossRef](#)]
39. Walas, M.; Lewandowski, T.; Synak, A.; Lapinski, M.; Sadowski, W.; Koscielska, B. Eu<sup>3+</sup> doped tellurite glass ceramics containing SrF<sub>2</sub> nanocrystals: Preparation, structure and luminescence properties. *J. Alloys Compd.* **2017**, *696*, 619–626. [[CrossRef](#)]
40. Han, Y.J.; Park, S.J. Hydrogen Storage Behaviors of Porous Carbons Derived from Poly(vinylidene fluoride). *J. Nanosci. Nanotechnol.* **2017**, *17*, 8075–8080. [[CrossRef](#)]
41. Wang, J.C.; Han, W.F.; Wang, S.C.; Tang, H.D.; Liu, W.C.; Li, Y.; Lu, C.S.; Zhang, J.J.; Kennedy, E.M.; Li, X.N. Synergistic catalysis of carbon-partitioned LaF<sub>3</sub>-BaF<sub>2</sub> composites for the coupling of CH<sub>4</sub> with CHF<sub>3</sub> to VDF. *Catal. Sci. Technol.* **2019**, *9*, 1338–1348. [[CrossRef](#)]



© 2020 by the authors. Licensee MDPI, Basel, Switzerland. This article is an open access article distributed under the terms and conditions of the Creative Commons Attribution (CC BY) license (<http://creativecommons.org/licenses/by/4.0/>).